JOURNAL OF COMPUTATIONAL PHYSICS 42, 53–76 (1981)

Study of Coating Flow by the Finite Element Method

H. SAITO* AND L. E. SCRIVEN

Department of Chemical Engineering & Materials Science, University of Minnesota, Minneapolis, Minnesota 55455

Received November 12, 1980

Silliman's analysis of slot coating is extended to accommodate film flows with highly bent menisci, as in slide and curtain coating, by combining polar and Cartesian coordinate parametrizations of meniscus shape. The nonlinear algebraic equations from the subdomain/Galerkin weighted residual method and finite element basis functions are solved by Newton's method, which is perfected for the free boundary problem. Convergence behavior is examined. Slot-coating results reveal slow-flow zones and show that at high capillary number and low metering rate the downstream meniscus can no longer attach to the slot. Comparison of Coyne and Elrod's approximate solutions with the finite element solutions shows that their assumption of a parabolic velocity profile leads to reasonable approximations of meniscus shapes.

1. INTRODUCTION

Viscous free-surface flows are important in coating technology, polymer processing, and other engineering applications as well as in certain areas of science. For understanding, designing and controlling such flow systems, computer-aided analysis by the finite element approach is very promising (Nickell *et al.* [12], Tanner *et al.* [27], Tanner [28], Orr and Scriven [14], Silliman and Scriven [20, 21, 24], Chang *et al.* [3]). This approach is a combination of the weighted residual methods of subdomains and of Galerkin, with simple basis functions that are designed for computational advantage. A curved free surface, or meniscus, by its presence generally makes the flow problem nonlinear whether or not curvilinear acceleration of the fluid does so too. Then the finite element approach reduces the mathematical problem of steady flow to a large set of simultaneous, nonlinear, algebraic equations. This set has to be solved iteratively.

Whether a given first approximation and chosen iteration process converge to a solution and, if they do, the rate of convergence, are matters crucial to the success of the finite element or any other discretization approach. Free surfaces raise special difficulties which until now have not been resolved. This paper addresses (i) the

* Present address: Fuji Photo Film Company Ltd., 210 Nakanuma, Minami-ashigara-shi, Kanagawa, Japan.

0021-9991/81/070053-24$02.00/0

Copyright © 1981 by Academic Press, Inc.
All rights of reproduction in any form reserved.

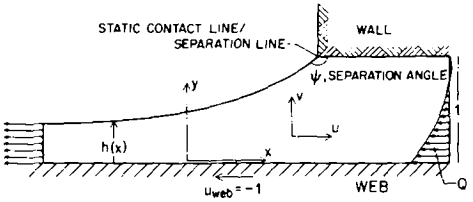

FIG. 1. Slot-coating flow with fixed contact line.

means of representing the free surface, and (ii) the application of Newton's iteration process to the algebraic equation set. The paper also reports results on flow out of a slot which go beyond the pioneering study by Silliman and Scriven [23,25].

We restrict consideration to steady, two-dimensional, viscous free-surface flow of an incompressible, Newtonian liquid carried out of a narrow slot by a moving substrate (Fig. 1). On the surface the boundary conditions are (1) the shear stress exerted by the adjacent gas phase is negligible, and (2) the normal stress, i.e., the pressure, exerted by the adjacent gas is balanced by the sum of the pressure and normal viscous stress exerted by the liquid and the capillary pressure in the surface itself (capillary pressure is the product of surface tension by twice the mean surface curvature). But the location of the free surface is unknown *a priori*, and so an additional boundary condition is relevant: (3) the surface is indeed the gas–liquid interface and velocity is continuous into that interface—the kinematic boundary condition. Within the liquid the governing equations are of course the continuity equation and the Navier–Stokes equation, suitably specialized (see below). Were the free surface not free, two boundary conditions would suffice at it. That there are three boundary conditions to be satisfied is one source of the difficulties that have been encountered.

Heretofore the iteration schemes used have been successive approximation techniques, types of functional iteration sometimes called Picard methods (Isaacson and Keller [9], Rheinboldt [15]). They proceed in a three-part cycle: (1) a free-surface shape is assigned; (2) a flow field within that shape is found from the Navier–Stokes equation system with one of the free-surface boundary conditions omitted, viz., the kinematic condition, the normal stress balance, or the vanishing of shear stress; (3) the free-surface shape is revised to satisfy as closely as possible the previously omitted boundary condition; (1) on the basis of the revision a new shape is assigned. If the process converges, the cycle is repeated until the desired convergence is achieved. Unfortunately the process does not always converge, regardless of which boundary condition is chosen for iteration, and regardless of the iteration scheme used in step 2. There was controversy about iterating on the kinematic condition (Tanner [28]) and normal stress condition (Orr and Scriven [14]) until Silliman and Scriven [23, 24] showed that when the capillary number $N_{Ca} \equiv \mu U/\sigma$, which measures the ratio of normal stress to capillary pressure, falls below unity, normal stress iteration converges well and kinematic iteration eventually fails, whereas as N_{Ca} rises beyond unity, the performances of the two iteration

schemes are reversed. Silliman [23] went on to demonstrate that it is possible to avoid Picard iteration and iterate on the full equation set, thereby finding the flow field and free-surface location simultaneously.

This demonstration made use of a variant of Newton's iteration process, which proved capable of converging at any value of N_{Ca}. However, the convergence rate was still highly dependent on the value of N_{Ca}, becoming excessively slow when $N_{Ca} > 10$.

In this paper we show that when the Jacobian matrix which is used in Newton iteration of the full equation set is calculated correctly, the convergence rate is strikingly improved; moreover, it becomes second order, or quadratic, as it proceeds, in accord with the asymptotic theory of the method (Isaacson and Keller [9]). In the variant employed in Silliman's demonstration, the derivatives with respect to free-surface location of those residuals that are area integrals were neglected. Such derivatives are required for any free-surface problem and so we have shown how to derive them in general, as reported in detail elsewhere (Saito and Scriven [19]).

A great attraction of Newton's process, besides rapid convergence when suitable first approximations can be generated, is the wealth of information contained in the Jacobian of the converged solution (Silliman and Scriven [22], Brown *et al.* [2]). Here we provide additional illustrations of the use of that information, i.e., sensitivity analysis and first-order continuation with respect to a parameter.

Whether Picard or Newton iteration is used, Silliman's computer code converges less and less well and then diverges as the dimensionless flow rate out of the slot is reduced. As that flow diminishes, the free surface bends more and more until the representation used in the code becomes singular. This type of difficulty with a representation is not uncommon in free-surface problems, and places a restriction on the range of parameter values that can be handled. In this paper we establish a method to avoid the difficulty by representing the free surface with a combination of different parametrizations of it, each of them the most convenient one for some part of it. In particular, we combine Cartesian-spine and radial-spine representations where Silliman's code made use of the former alone. This approach, which should be simpler than Ruschak's [17] general spine version, like it greatly enlarges the range of accessible parameter values and is applicable to a variety of flow problems.

2. Original Mathematical Formulation

The weak form of the Navier–Stokes and continuity equations for steady, two-dimensional, incompressible Newtonian flow is well established and the finite element version follows immediately. The basis, or interpolation, functions are chosen for expanding the component velocities, which here we take to be Cartesian components, the pressure, and the location of the free surface, or meniscus (Silliman and Scriven [24]):

$$u = \sum u_i \bar{\phi}^i(\mathbf{r}), \quad v = \sum v_i \bar{\phi}^i(\mathbf{r}), \quad p = \sum p_i \bar{\psi}^i(\mathbf{r}), \quad h = \sum h_i \bar{\chi}^i(\mathbf{r}_{11}, \mathbf{r}), \qquad (1)$$

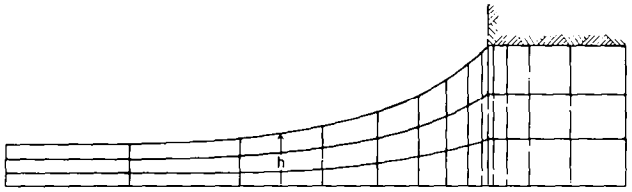

FIG. 2. Silliman's tessellation of the flow domain for the slot-coating problem. The vertical scale is exaggerated by a factor of 2.

where $\mathbf{r}$ is the position vector and $\mathbf{r}_{II}$ is that of a suitably chosen reference surface from which distance h to the free surface is measured. The basis functions $\bar{\phi}^i$, $\bar{\psi}^i$ and $\bar{\chi}^i$ are to be distinguished from their counterparts $\phi^i(\xi, \eta)$, $\psi^i(\xi, \eta)$, and $\chi^i(\xi)$ in the (ξ, η) domain introduced below. Each basis function is nonzero only on the subdomain consisting of elements contiguous to its node. Figure 2 shows a typical tessellation. The elements are defined by spines of constant x and curved sides are so located that the thicknesses of successive ranks of elements are in constant ratios to the distance between the free surface and the web. For convenience each curvilinear (x, y)-element is mapped isoparametrically into the fixed (ξ, η)-domain as shown in Fig. 3; then (Strang and Fix [26])

$$\begin{aligned} x &= \sum X_i \phi^i(\xi, \eta), & y &= \sum Y_i \phi^i(\xi, \eta), \\ u(x, y) &= \sum u_i \phi^i(\xi, \eta), & v(x, y) &= \sum v_i \phi^i(\xi, \eta), \\ p(x, y) &= \sum p_i \psi^i(\xi, \eta), & h(x) &= \sum h_i \chi^i(\xi), \end{aligned} \tag{2}$$

where X_i and Y_i are the coordinates of the ith node in an element.

Following Silliman [23] we employ conventional "mixed interpolation" with nine-node quadratic basis functions ϕ^i for velocity, four-node bilinear ones ψ^i for pressure, and Hermite cubic ones χ^i for free-surface location. (In the cubic elements separate functions are associated with h and its derivative at each node: cf. Strang and Fix [26].) With body forces put aside, the momentum equations are

$$\begin{aligned} \mathbf{M}_i &\equiv \int_A \phi^i(-\nabla \cdot \mathbf{T} + N_{Re}\mathbf{u} \cdot \nabla \mathbf{u})\, dA \\ &\equiv \int_A (\nabla \phi^i \cdot \mathbf{T} + \phi^i N_{Re}\mathbf{u} \cdot \nabla \mathbf{u})\, dA - \oint_{\partial A} \phi^i \mathbf{n} \cdot \mathbf{T}\, ds = \mathbf{0}, \end{aligned} \tag{3}$$

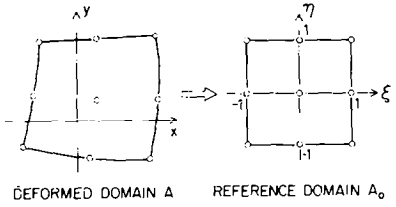

FIG. 3. Isoparametric mapping, i.e., mapping by the polynomial function of the finite element itself.

where the stress tensor is $\mathbf{T} = -p\mathbf{1} + [\nabla\mathbf{u} + (\nabla\mathbf{u})^T]$, ∂A is the boundary of the flow domain A, and $N_{Re} \equiv Ud/\nu$. $\mathbf{M}_i$ is the momentum residual, which vanishes when the requirement of momentum conservation is met. The variables are all dimensionless, length being measured in units of gap width d, velocities in units of web speed U, and pressures in units of $\rho\nu U/d$, where ρ is density and ν is kinematic viscosity. On the boundaries, $\mathbf{n}$ and $\mathbf{t}$ are the unit normal and tangent; in terms of $h(x)$:

$$\begin{pmatrix} \mathbf{n} \\ \mathbf{t} \end{pmatrix} = \frac{1}{\sqrt{1+h_x^2}} \begin{pmatrix} -h_x\mathbf{i} + \mathbf{j} \\ \mathbf{i} + h_x\mathbf{j} \end{pmatrix},$$

where $\mathbf{i}$ and $\mathbf{j}$ are unit vectors in x- and y-directions. The traction $\mathbf{n} \cdot \mathbf{T}$ in (3) can be decomposed into normal and tangential parts to use later in the boundary conditions at the free suface: thus

$$\mathbf{M}_i = \int_A (\nabla\phi^i \cdot \mathbf{T} + \phi^i N_{Re}\mathbf{u} \cdot \nabla\mathbf{u})\, dA - \oint_{\partial A} \phi^i(\mathbf{nnn} : \mathbf{T} + \mathbf{tnt} : \mathbf{T})\, ds = \mathbf{0}. \tag{4}$$

The continuity equations are

$$C_i \equiv \int_A \psi^i \nabla \cdot \mathbf{u}\, dA = 0, \tag{5}$$

C_i is the mass residual, which vanishes when the requirement of mass conservation is met.

At the inlet the velocity distribution is fully developed Couette–Poiseuille flow $g(y)$ that satisfies no-slip conditions on the web and the wall, i.e., $g(0) = -1$ and $g(1) = 0$. The net flow is $Q = \int g\, dy$. At the outlet there is supposed to be no diffusive outflow of momentum. Thus the boundary conditions, apart from those on the free surface, are

$$\begin{array}{lll} \text{At the inflow} & \mathbf{n} \cdot \mathbf{u} = g(y), & \mathbf{t} \cdot \mathbf{u} = 0, \\ \text{At the outflow} & \mathbf{nn} : \mathbf{T} = 0, & \mathbf{t} \cdot \mathbf{u} = 0, \\ \text{On the wall} & \mathbf{n} \cdot \mathbf{u} = 0, & \mathbf{t} \cdot \mathbf{u} = 0, \\ \text{On the web} & \mathbf{n} \cdot \mathbf{u} = 0, & \mathbf{t} \cdot \mathbf{u} = -1. \end{array} \tag{6}$$

Of these, all except $\mathbf{nn} : \mathbf{T} = 0$ at the outlet are essential boundary conditions. At the free surface, following Silliman, we take the kinematic condition as an essential one and the shear stress condition as a natural one:

$$\text{At the free surface} \qquad \mathbf{n} \cdot \mathbf{u} = 0, \qquad \mathbf{nt} : \mathbf{T} = 0. \tag{7}$$

This choice leaves the normal stress condition autonomous among the free-surface boundary conditions, i.e., its residual is to be made orthogonal to the basis functions defining the position of the free surface. Elsewhere we have shown [18] that in the

case of the die swell problem this is superior to choosing either the kinematic or the shear stress boundary condition as the autonomous one.

In the Galerkin or weak form the normal stress boundary condition is

$$F_i \equiv \int_{s_*} \chi^i (2H - N_{Ca}\mathbf{nn} : \mathbf{T})\, ds_* = 0, \tag{8}$$

where the surface tension σ of the liquid is in $N_{Ca} \equiv \mu U/\sigma$, H is the mean curvature of the free surface and the integration is defined on a reference surface s_*—here its profile, the x-axis—for the purpose of integrating the curvature term by parts later. Ambient pressure is set to zero as the datum for the pressure. The mean curvature is defined as $H \equiv -\frac{1}{2}\nabla_s \cdot \mathbf{n}$, where ∇_s is the surface gradient operator on the free surface. For the Cartesian parametrization,

$$2H \equiv -\nabla_s \cdot \mathbf{n} = -\nabla_* \cdot \mathbf{n} = \frac{d}{dx}\left(\frac{h_x}{\sqrt{1+h_x^2}}\right), \tag{9}$$

where ∇_* is a gradient on the planar reference plane ($\mathbf{i}(\partial/\partial x)$ in the two-dimensional case here) (Orr [13]). Thus with the surface divergence theorem (Weatherburn [29]) Eq. (8) becomes

$$\begin{aligned} F_i &= \int_{s_*} (\mathbf{n} \cdot \nabla_* \chi^i - \chi^i N_{Ca}\mathbf{nn} : \mathbf{T})\, ds_* - \int_{\partial s_*} \chi^i \mathbf{n} \cdot \mathbf{m}_s\, ds \\ &= \int_{x_1}^{x_2} \left(-\chi_x^i \frac{h_x}{\sqrt{1+h_x^2}} - \chi^i N_{Ca}\mathbf{nn} : \mathbf{T}\right) dx \\ &\quad + \left[\chi^i \frac{h_x}{\sqrt{1+h_x^2}}\right]_{x_1}^{x_2} = 0, \end{aligned} \tag{10}$$

where $\mathbf{m}_s$ is the outward pointing normal vector on the boundary s_* and x_1 and x_2 are x-coordinates at the end points of the free-surface profile. Formulation (10) derived from (8) and (9) by the divergence theorem (equivalently integration by parts in the two-dimensional case here) is quite convenient, because (i) lower-order basis functions can be used for the free surface since Eq. (10) contains only first-order derivatives with respect to x instead of the original second-order derivatives in $2H$, and (ii) boundary conditions on the slope at the end points can be easily introduced as natural boundary conditions. Boundary conditions for the free-surface position are the fixed separation line at the edge of the slot exit, an essential boundary condition; and vanishing slope at the downstream section, a natural boundary condition:

$$\begin{aligned} &\text{At the separation line} \qquad h = 1, \\ &\text{At the outflow section} \qquad h_x = 0. \end{aligned} \tag{11}$$

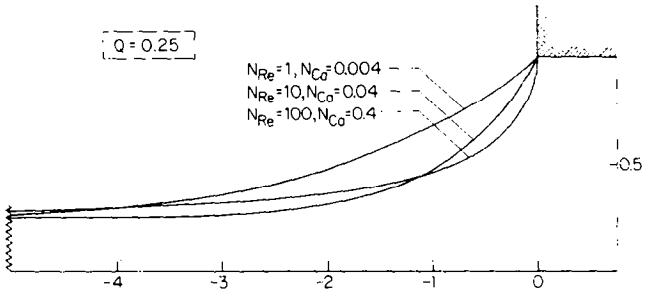

FIG. 4. Dependence of meniscus profile on Reynolds number N_{Re}, and capillary number, N_{Ca}, according to Silliman's code [23]. The vertical scale is exaggerated by a factor of 2.

In Silliman's code the x-component of (4), simplified with (7), is retained for elements adjoining the free surface:

$$M_i^x \equiv \mathbf{i} \cdot \mathbf{M}_i = 0 \tag{12}$$

and the y-component there is replaced by the kinematic condition at free-surface nodes of the tessellation,

$$K_i \equiv \mathbf{n}^i \cdot \mathbf{u} = 0. \tag{13}$$

The finite element equations are the following set of nonlinear algebraic equations: x- and y-components of (3) when ϕ^i belongs to any interior node; x-components of (3) with natural boundary conditions (6) at the outflow; (12) and (13) along free-surface sides of elements adjacent to the free surface; (5) for every pressure node; and (10) for free-surface nodes except at those where boundary conditions (11) are imposed. This set is solved simultaneously by Newton's iteration process in Silliman's code.

Among many calculations with the code we found convergence difficulties mounting as web speed was upped and N_{Re} and N_{Ca} grew large at fixed flow rate Q. Figure 4 shows the progression of free-surface shapes. As meniscus inclination at the separation line (static contact line) approached vertical, i.e., $dh/dx \to \infty$, convergence worsened: indeed the code could not calculate any case in which the meniscus enters the slot. We found the same behavior when we diminished Q at fixed N_{Re} and N_{Ca}. Because high web speed and low flow rates are quite important in practice, we sought to overcome the difficulty, which can be traced to singularity of the Jacobian in Newton's method when the meniscus is nearly vertical.

3. Reformulation with Combined Free-Surface Representations

A simple way to avoid the difficulty is to represent the free surface near the separating contact line with a polar coordinate parametrization $f(\theta)$, where θ is an azimuthal angle. On one of the radial spines through the polar center this

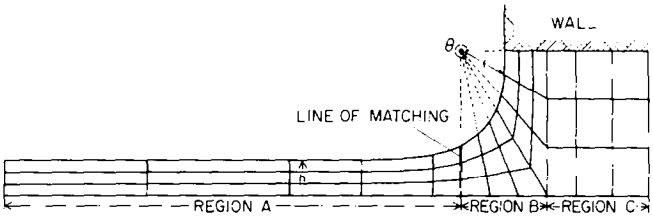

FIG. 5. Combined tessellation of the low domain for the slot-coating problem. The vertical is exaggerated by a factor of 2.

parametrization must be matched with the Cartesian-spine representation downstream, and the elements beneath the highly curved meniscus must be matched to those beneath the less curved meniscus downstream. Also, there must be suitable matching with rectangular elements upstream when they are employed, as they are here.

Figure 5 illustrates the idea with a tessellation in which the position of the free surface, or meniscus, in Region B is represented by the polar arm of length $f(\theta)$ and in Region A it is represented in the usual way by height $h(x)$ above the web. The two representations join at the matching line.

In the finite element formulation the expansions at Eqs. (1) and (2) remain unchanged except that

$$\begin{aligned} h(x) &= \sum h_i \chi^i(\xi) \qquad \text{in Region A,} \\ f(\theta) &= \sum f_i \chi^i(\theta) \qquad \text{in Region B,} \end{aligned} \tag{14}$$

$$\mathbf{G} = \begin{pmatrix} h(x) - 1 + f(\theta) \\ h_x f - f_0 \end{pmatrix} = \mathbf{0} \qquad \text{at the matching point } P_0 \text{ in Fig. 6.} \tag{15}$$

Equations (15) guarantee continuity of the two-piece surface representation and of its slope.

In the original formulation the assembled subdomain momentum equations associated with free-surface nodes were resolved into x- and y-components and the latter were replaced by kinematic conditions at Eqs. (12) and (13). This procedure we

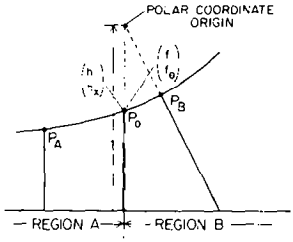

FIG. 6. Double-point of the free surface, where the two coordinate parametrizations are matched.

found to break down, as expected, when at any point on the free surface the tangent approaches the direction of the y-axis. A logical procedure from the standpoint of taking the vanishing of shear stress as a natural boundary condition and leaving the normal stress balance as the autonomous one is to resolve the momentum equations into tangential and normal components and to replace the normal components by the kinematic conditions. Thus Eq. (12) is replaced by

$$M_i^t \equiv \mathbf{t} \cdot \mathbf{M}_i = 0. \tag{16}$$

The normal and tangent along the free surface are

$$\begin{aligned}
\begin{pmatrix} \mathbf{n} \\ \mathbf{t} \end{pmatrix} &= \frac{1}{\sqrt{1+h_x^2}} \begin{pmatrix} -h_x\mathbf{i}+\mathbf{j} \\ \mathbf{i}+h_x\mathbf{j} \end{pmatrix} \qquad \text{in Region A,} \\
\begin{pmatrix} \mathbf{n} \\ \mathbf{t} \end{pmatrix} &= \frac{1}{\sqrt{f^2+f_\theta^2}} \begin{pmatrix} -f\mathbf{e}_r + f_\theta \mathbf{e}_\theta \\ f_\theta \mathbf{e}_r + f\mathbf{e}_\theta \end{pmatrix} \\
&= \frac{1}{\sqrt{f^2+f_\theta^2}} \begin{pmatrix} a\mathbf{i}+b\mathbf{j} \\ b\mathbf{i}-a\mathbf{j} \end{pmatrix} \qquad \text{in Region B,}
\end{aligned} \tag{17}$$

where $\mathbf{e}_r$ and $\mathbf{e}_\theta$ are unit vectors in the r- and θ-directions and $a \equiv -f\cos\theta - f_\theta \sin\theta$ and $b \equiv -f\sin\theta + f_\theta\cos\theta$. The results described below confirm that this procedure avoids the earlier difficulty and leads to correct solutions.

In terms of polar coordinates the curvature of a two-dimensional surface is

$$2H = -\nabla_s \cdot \mathbf{n} = -\frac{1}{f}\nabla_* \cdot \mathbf{n} = \frac{1}{\sqrt{f^2+f_\theta^2}} - \frac{1}{f}\frac{1}{d\theta}\left(\frac{f_\theta}{\sqrt{f^2+f_\theta^2}}\right), \tag{18}$$

where the reference surface is taken to be a unit circle and the surface gradient ∇_* on the reference surface is $\nabla_* \equiv \mathbf{e}_\theta \partial/\partial\theta$ (Orr [13]). The Galerkin or weak form of the normal stress boundary condition is defined as

$$F_i \equiv \int_{s_*} \chi^i (2H - N_{Ca}\mathbf{nn} : \mathbf{T})\, f\, ds_* = 0, \tag{19}$$

where s_* is a unit radius reference circle and f is a weighting function introduced for convenience in integrating the curvature term by parts. Then with (18) and the surface divergence theorem (Weatherburn [29]), Eq. (19) becomes

$$\begin{aligned}
F_i &= \int_{s_*} (\mathbf{n}\cdot\nabla_*\chi^i + \chi^i(2H)_*\mathbf{n}\cdot\mathbf{n}_* - \chi^i N_{Ca}\mathbf{nn} : \mathbf{T}f)\, ds_* - \int_{\partial s_*} \chi^i \mathbf{n}\cdot\mathbf{m}_s\, ds \\
&= \int_{\theta_1}^{\theta_2} \left(\frac{f_\theta \chi_\theta^i + f\chi^i}{\sqrt{f^2+f_\theta^2}} - N_{Ca}\chi^i \mathbf{nn} : \mathbf{T}f\right) d\theta - \left[\chi^i \frac{f_\theta}{\sqrt{f^2+f_\theta^2}}\right]_{\theta_1}^{\theta_2},
\end{aligned} \tag{20}$$

where $(2H)_*$ is the curvature of the reference surface, i.e., unity in this case; and $\mathbf{n}_*$ is a unit normal to the reference surface, i.e., $\mathbf{n}_* = \mathbf{e}_r$. Integrating the curvature term by parts in (19) is also possible with a constant weighting function as Orr [13] showed, but integration on a suitable reference surface is essential to the simplification attendant on integration by parts. The boundary conditions for the free-surface position are the same as before:

$$\begin{aligned} &\text{At the separation line} && f = \text{constant}, \\ &\text{At the outflow section} && h_x = 0. \end{aligned} \tag{21}$$

At the matching point P_0 in Figs. 5 and 6 it is convenient to have four unknowns, two associated with the pair of Hermite cubic polynomial basis functions in the surface element to the left, and two associated with the one to the right. Besides the two matching conditions at Eq. (15), there are two normal stress equations associated with the matching point:

$$\begin{aligned} F_i &\equiv \int_{P_A}^{P_0} \chi^i(x)(2H - N_{Ca}\mathbf{nn} : \mathbf{T})\, dx + \int_{P_0}^{P_B} \chi^i(\theta)(2H - N_{Ca}\mathbf{nn} : \mathbf{T}) f\, d\theta \\ &= \int_{P_A}^{P_0} \left(-\chi^i_x(x) \frac{h_x}{\sqrt{1+h_x^2}} - \chi^i N_{Ca}\mathbf{nn} : \mathbf{T} \right) dx + \left[\chi^i \frac{h_x}{\sqrt{1+h_x^2}} \right]_{x_A}^{x_0} \\ &\quad + \int_{P_0}^{P_B} \left(\frac{\chi^i_\theta f_\theta + \chi^i f}{\sqrt{f^2 + f_\theta^2}} - \chi^i N_{Ca}\mathbf{nn} : \mathbf{T} f \right) d\theta - \left[\chi^i \frac{f_\theta}{\sqrt{f^2 + f_\theta^2}} \right]_{\theta_0}^{\theta_B} \\ &= 0, \end{aligned} \tag{22}$$

where i takes on values 1 and 2 corresponding to the basis functions of the Hermite cubics at the matching node.

Inside the flow domain of Region B a polar parametrization could be used, in which case there would be a set of matching conditions at the interior nodes along the matching line. However, there appears to be no advantage in using a polar parametrization there: it would merely alter weightings in the isoparametric mappings into the fixed (ξ, η)-domain. Hence we retain the Cartesian parametrization throughout the interior.

It is easy to confirm that the new formulation becomes exactly the same as the original, ordinary one when the coordinate systems used to parametrize Regions A and B are the same. It is also not hard to see how to combine other free-surface representations to advantage for other free-surface problems.

4. Newton Iteration for the Reformulation

The set of nonlinear algebraic equations consists of x- and y-components of momentum equations (3) for the interior nodes; x-components of (3) with natural boundary conditions (6) at the outlet; (16) and (13) along free-surface sides of

elements adjacent to the free surface; (5) for every pressure node; (19) for free-surface nodes except for boundary condition (20) nodes and matching point P_0; and (15) and (22) for the matching point P_0. The set can be written in terms of a vector of residuals $\mathbf{R} \equiv \{\mathbf{M}_i, C_i, K_i, F_i, \mathbf{G}\}$:

$$\mathbf{R}(\boldsymbol{\alpha}, \boldsymbol{\beta}) = \mathbf{0}, \tag{23}$$

where $\boldsymbol{\alpha} \equiv \{u_i, v_i, p_i\}$ and $\boldsymbol{\beta} \equiv (h_i, f_i\}$. Then the well-known Newton process is

$$\begin{pmatrix} \boldsymbol{\alpha}_{n+1} \\ \boldsymbol{\beta}_{n+1} \end{pmatrix} = \begin{pmatrix} \boldsymbol{\alpha}_n \\ \boldsymbol{\beta}_n \end{pmatrix} - \mathbf{J}^{-1}\mathbf{R}(\boldsymbol{\alpha}_n, \boldsymbol{\beta}_n), \tag{24}$$

where $\mathbf{J} \equiv (\partial\mathbf{R}/\partial\boldsymbol{\alpha}, \partial\mathbf{R}/\partial\boldsymbol{\beta})$. Now, in this Jacobian matrix the components of $\partial\mathbf{R}/\partial\boldsymbol{\alpha}$ arise in any fixed boundary flow problem and there is no difficulty in calculating them. The difficulty in free-surface problems has been the accurate calculation of the components of $\partial\mathbf{R}/\partial\boldsymbol{\beta}$, i.e., sensitivities of all the residuals throughout the flow domain to the location and the shape of the meniscus, as given by the position of the free-surface nodes of the tessellation.

The residuals (apart from the K_i and $\mathbf{G}$) are expressed by volume and area integrals in the x–y plane. The integrands are functions of the coordinates x and y and of the nodal values $\boldsymbol{\alpha}$ and $\boldsymbol{\beta}$ in the finite element expansions. However, because $\boldsymbol{\beta}$ determines the shapes of all of the elements except those within the slot, x and y in most of the integrands depend on $\boldsymbol{\beta}$, a quite troublesome feature.

Especially tough is the evaluation of derivatives for the Jacobian matrix, because the residuals of the momentum and continuity equations depend on $\boldsymbol{\beta}$ not only through the integrands but also through the limits of integration, i.e., the element domains. In the original formulation, Silliman sidestepped this difficulty by assuming that the volume area integral terms do not depend on $\boldsymbol{\beta}$ through the element domains, on the grounds that the dependence ought to disappear as the continuity and Navier–Stokes equations come to be well satisfied locally. This assumption approximates more closely the truth as $\boldsymbol{\alpha}_n$ and $\boldsymbol{\beta}_n$ approach a solution, but can be far from correct in the early stages of an iteration. Computational tests with the original code revealed that the rate of convergence with this approximation is highly sensitive to parameter values (N_{Re}, N_{Ca}, and Q) and seldom approaches the quadratic asymptotic convergence that is characteristic of Newton iteration (cf. Fig. 17 below).

This difficulty can be overcome by correctly evaluating the derivatives in the Jacobian. The volume (area) integral terms can be handled properly with the general transport theorem, or entirely equivalently with the following scheme which is couched in terms of the isoparametric mappings of elements into the fixed (ξ, η)-domain (Saito and Scriven [19]), as shown in Fig. 3. With the transformation $(x, y) \rightarrow (\xi, \eta)$ given by Eq. (2), where the coordinates $X_i(\boldsymbol{\beta})$, $Y_i(\boldsymbol{\beta})$ of the ith node of an element depend on the free-surface location $\boldsymbol{\beta}$, an area integral from a two-dimensional flow,

$$I(\boldsymbol{\alpha}, \boldsymbol{\beta}) = \int_{A(\boldsymbol{\beta})} F(x, y, \boldsymbol{\alpha}, \boldsymbol{\beta})\, dA \tag{25}$$

can be expressed as

$$I(\alpha, \beta) = \int_{A_0} F(x(\xi, \eta; \beta), y(\xi, \eta; \beta), \alpha, \beta) \, |\mathscr{J}| \, d\xi \, d\eta, \tag{26}$$

where $\mathscr{J}$ is the Jacobian of the transformation, viz.,

$$\mathscr{J} \equiv \left[\frac{\partial(x, y)}{\partial(\xi, \eta)}\right] \equiv \begin{bmatrix} \partial x/\partial \xi & \partial x/\partial \eta \\ \partial y/\partial \xi & \partial y/\partial x \end{bmatrix}. \tag{27}$$

If the integrand F in Eq. (25) contains $\partial/\partial x$ or $\partial/\partial y$ these operators are transformed by

$$\begin{aligned} \frac{\partial}{\partial x} &= \frac{\partial \xi}{\partial x}\frac{\partial}{\partial \xi} + \frac{\partial \eta}{\partial x}\frac{\partial}{\partial \eta}, \\ \frac{\partial}{\partial y} &= \frac{\partial \xi}{\partial y}\frac{\partial}{\partial \xi} + \frac{\partial \eta}{\partial y}\frac{\partial}{\partial \eta}, \end{aligned} \tag{28}$$

where the coefficients can be extracted from

$$\begin{bmatrix} \partial \xi/\partial x & \partial \xi/\partial y \\ \partial \eta/\partial x & \partial \eta/\partial y \end{bmatrix} = \mathscr{J}^{-1} = \frac{1}{|\mathscr{J}|}\begin{bmatrix} \partial y/\partial \eta & -\partial x/\partial \eta \\ -\partial y/\partial \xi & \partial x/\partial \xi \end{bmatrix}. \tag{29}$$

Thus the integrand $F\,|\mathscr{J}|$ in Eq. (26) can be completely freed of dependence on the original coordinates. The domain of integration A_0 is the fixed square, and ξ and η are independent of β. Hence the needed derivative is simply

$$\frac{\partial I}{\partial \beta} = \int_{A_0} \frac{\partial}{\partial \beta}\left(F(\xi, \eta, \alpha, \beta)\,|\mathscr{J}|\right) d\xi \, d\eta \tag{30}$$

and this is easily enough worked out analytically.

The line integrals occurring in the momentum equations (3) and normal stress conditions (19) and (22) can be handled similarly. By converting from arc length ds to

$$\begin{aligned} dx &= (1 + h_x^2)^{-1/2} \, ds \qquad \text{in Region A}, \\ d\theta &= (f^2 + f_\theta^2)^{-1/2} \, ds \qquad \text{in Region } B \end{aligned} \tag{31}$$

the limits of integration become fixed values of β and the line integrals take the form

$$\begin{aligned} L(\alpha, \beta) &= \int_{x_n}^{x_{n+1}} \mathscr{B}(x, y(x; \beta), \alpha, \beta) \, dx \qquad \text{in Region A} \\ &= \int_{\theta_n}^{\theta_{n+1}} \mathscr{C}(x(\theta; \beta), y(\theta; \beta), \alpha, \beta) \, d\theta \qquad \text{in Region B}. \end{aligned} \tag{32}$$

When these are mapped to the ξ–η domain they become

$$\begin{aligned} L(\alpha, \beta) &= \int_{-1}^{1} \mathscr{B}(\xi, \eta = 1, \alpha, \beta) \frac{x_{n+1} - x_n}{2} d\xi \qquad \text{in Region A} \\ &= \int_{\theta_n}^{\theta_{n+1}} \mathscr{C}(\xi(\theta), \eta = 1, \alpha, \beta)\, d\theta \qquad \text{in Region B.} \end{aligned} \tag{33}$$

The needed derivatives with respect to β are then

$$\begin{aligned} \frac{\partial L}{\partial \beta} &= \int_{-1}^{1} \frac{\partial \mathscr{B}(\xi, 1, \alpha, \beta)}{\partial \beta} \frac{x_{n+1} - x_n}{2} d\xi \qquad \text{in Region A} \\ &= \int_{\theta_n}^{\theta_{n+1}} \frac{\partial \mathscr{C}(\xi(\theta), 1, \alpha, \beta)}{\partial \beta} d\theta \qquad \text{in Region B,} \end{aligned} \tag{34}$$

where $\xi(\theta)$ describes the mapped surface points, which lie along $\eta = 1$.

The details of implementing Newton iteration with the correct Jacobian based on

5. New Results for Slot-Coating Flow

The new formulation, with many borrowings from Silliman's code, was programmed for the CDC CYBER 74/172 at the University of Minnesota. The tesellation used is shown in Fig. 5. There are 42 elements, 203 velocity nodes, 60 pressure nodes and 23 free-surface nodes. The number of unknowns is 512. The Frontal routine (Hood [8]) was used to solve the simultaneous linear equation set. The amount of core memory required in the whole program was about 60K octal words, and the amount of out-of-core memory for the Frontal routine, originally designated for disc memory, was about 150K octal words. Around 8 sec were needed for one iteration.

Full Newton iteration was used, as outlined in the preceding section. The convergence criterion was normally that the maximum change in nodal values of velocity, pressure and free-surface coordinate be less than 10^{-4} (the criterion was tightened only during studies of convergence rate). The nearest available solution was ordinarily used for the first approximation with a new set of parameters; first-order continuation was sometimes used, as mentioned below. When the convergence criterion was not reached in six iterations, the change in parameter was decreased; the parameter changes were usually such that convergence was reached in five iterations. The parameter range investigated was $0 \leqslant N_{Re} \leqslant 400$, $0.01 \leqslant N_{Ca} \leqslant 20$ and $0.12 \leqslant Q \leqslant 0.5$. When the flow rate Q is so low, or the capillary number N_{Ca} so high, that the separation angle is less than about 20°, the corner element adjoining the separation line grows so deformed as to make the result unreliable in its neighborhood. This is the chief limitation on the parameter range. As to Reynolds

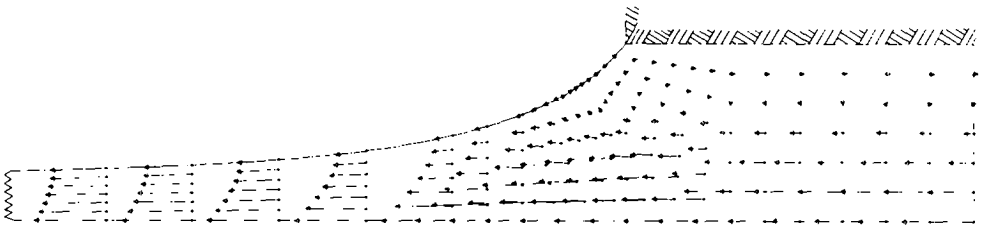

FIG. 7. Slot-coating flow with non-invading meniscus. $N_{Re} = 50$, $N_{Ca} = 0.125$, $Q = 0.25$ and $\psi = 129.9°$.

number, there were no difficulties in calculation up to $N_{Re} = 400$, the highest value attempted so far.

Calculated free surfaces and fields of velocity vectors are plotted in Fig. 7, an example of a non-invading meniscus, and in Fig. 8, an example of an invading one. The former agrees with Silliman's result based on the original formulation where nodes coincide. Features of particular interest in both bases are the extent and strength of recirculating flow, the separation angle ψ (cf. Fig. 1) at the corner where the contact line is fixed to the solid, the location of the stagnation line on the free surface, and the length of the transition zone in which the flow relaxes into its asymptotic uniform velocity state and the free surface relaxes to its asymptotic height above the moving web.

The relaxation is predicted to be exponential by Higgins' theory [6], which gives the relaxation rates sufficiently far downstream in terms of N_{Re}, N_{Ca}, and Q. Depending on the combination of these parameters, the asymptotic behavior of the meniscus is reached in a distance of a few tenths of the slot width to twice the slot width. Figure 9 shows the agreement of the finite element results and the asymptotic theory.

The shape of the meniscus near the separating line is a tougher problem. When capillary number N_{Ca} is much less than unity, it has often been approximated as a static meniscus (Landau and Levich [11], Ruschak [16], Higgins and Scriven [10]). We will discuss the validity of this assumption later, at Fig. 14. Here we illustrate in Figs. 10–12 how meniscus shape depends on the parameters, and in Figs. 13a–c how the angle of separation ψ and the mean curvature $1/r$ near the contact line change as the parameters vary. The separation angle is the angle between the normal to the slot wall and the normal to the free surface at the contact line (thus it is a type of contact

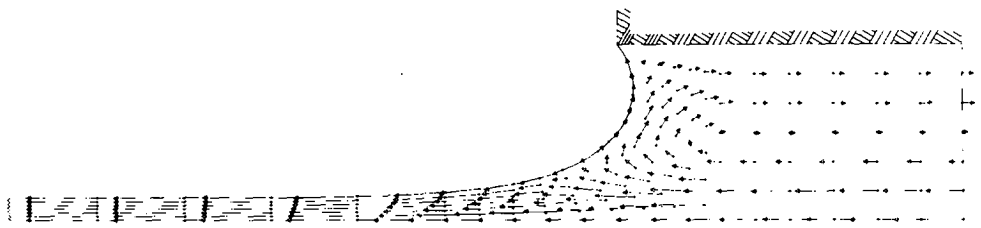

FIG. 8. Slot-coating invading meniscus. $N_{Re} = 50$, $N_{Ca} = 0.125$, $Q = 0.13$ and $\psi = 50.7°$.

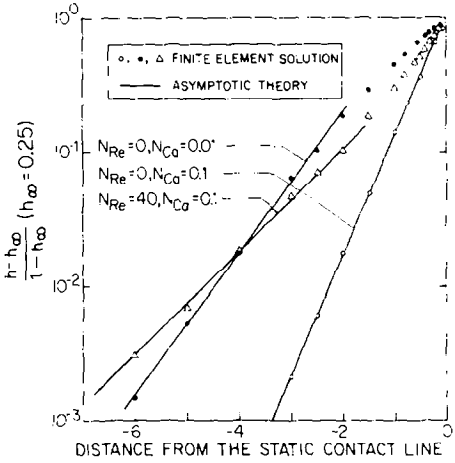

FIG. 9. Decay of film height downstream from the slot exit. Straight lines are predictions of Higgins' [6] asymptotic theory.

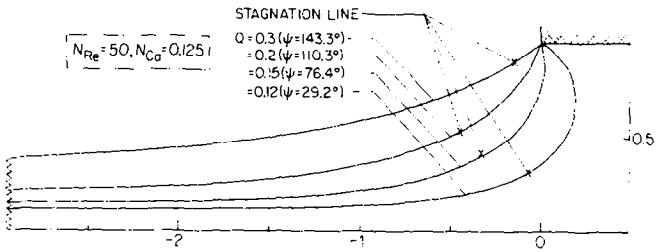

FIG. 10. Dependence of meniscus profile on dimensionless flow rate, Q.

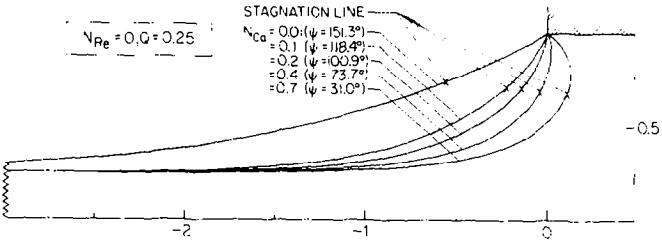

FIG. 11. Dependence of meniscus profile on capillary number, N_{Ca}.

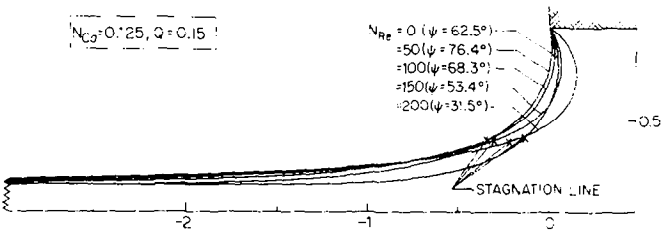

FIG. 12. Dependence of meniscus profile on Reynolds number, N_{Re}.

angle). The mean curvature, which can be regarded as the reciprocal of a radius of curvature r, is evaluated as the arithmetic average of the curvatures at the free-surface nodes in the element that abuts the contact line.

It is evident from Figs. 10, 11, 13a and b that as dimensionless flow rate Q decreases or capillary number N_{Ca} increases, the separation angle ψ falls and the mean curvature $1/r$ rises: the meniscus tends to invade the slot and the film to relax in a shorter distance downstream. The effect of Reynolds number N_{Re} is more complicated. As it increases, the rate of meniscus relaxation falls, as seen in Fig. 12, but neither the separation angle nor the mean curvature changes monotonically, as seen in Fig. 13c. How to interpret the maximum and the minimum is not clear yet.

All of the results make it plain that the separation angle falls as Q decreases or N_{Ca} increases. Generally the smaller the separation angle, the less the tendency for the meniscus to be pinned to the corner at the slot exit (down to 20°, at least, where the finite element solution becomes locally unreliable, as pointed out above). It appears that there is a critical separation angle—it might be as low as 0°—which is dictated by wetting behavior of the liquid on the slot wall and below which the meniscus no longer attaches to the corner at the slot exit. Such a limit would be crucial to the slot-coating process (the sensitivity analysis in the next section provides more information). That slot width puts a bound on meniscus curvature was already deduced by Ruschak [16] (cf. Higgins and Scriven [7]) with a quasi-static approximation, i.e., the meniscus shape is an arc of circle having a constant curvature predicted by Landau and Levich's [11] approximation. In other words, the radius of

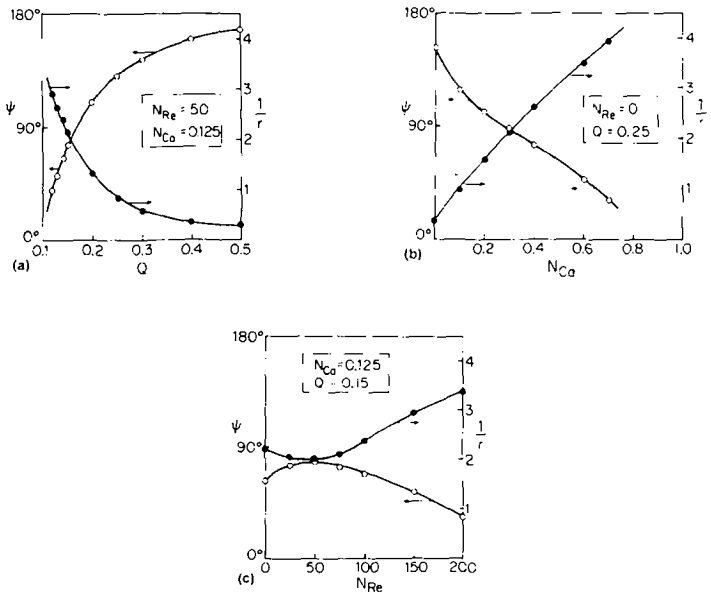

FIG. 13. Dependence of separation angle, ψ, and local curvature near separation, $1/r$, on (a) dimensionless flow rate, Q, (b) capillary number, N_{Ca}, and (c) Reynolds number, N_{Re}.

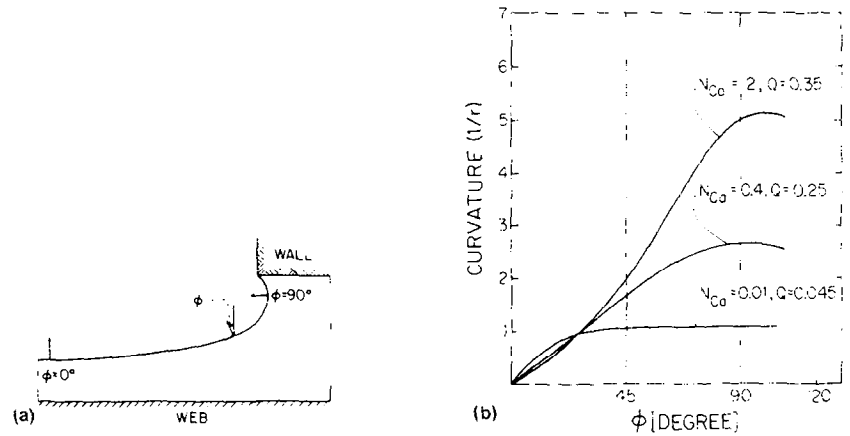

FIG. 14. (a) The definition of inclination ϕ. (b) the variation of curvature versus inclination, ϕ, along the free surface for zero Reynolds number.

curvature cannot be less than $(d - h_\infty)/2$, where d is gap width and h_∞ is a final thickness, and the separation angle is 0° in the limiting situation. The variation of curvature along the free surface is shown in Fig. 14b. The abscissa is the angle of inclination of the normal to the free surface from the y-direction, as depicted in Fig. 14a. Plainly, a large portion of the meniscus has constant curvature when capillary number, N_{Ca} , is very small; but the curvature varies more and more rapidly as N_{Ca} increases. This means that the assumption of Ruschak and Higgins and Scriven is reasonable when N_{Ca} is very small, but is less and less correct and their criteria are increasingly overstrict as N_{Ca} increases. The limit predicted here by finite element analysis has the same physical origin as the simple quasi-static approximation but takes account of dynamic effects and is accurate as long as the critical separation angle is more than 20°. However, a more refined analysis may be necessary when the critical separation angle is less than 20°. Although the curvature changes along the free surface in Fig. 14b, it is nearly constant between the most upstream place of the meniscus, where $\phi = 90°$, and the separation line. In an interesting attempt to approximate the effect of viscous stress on the meniscus, Coyne and Elrod [4] calculated an entire meniscus shape by assuming that the separation angle ψ is 90° and the velocity along spines perpendicular to the meniscus is parabolic up to the separation line. Their results include the ratios d/h_∞ and r_c/d as functions of $N \equiv (3N_{Ca})^{1/3}$, where d and h_∞ are as defined above, and r_c is the radius of meniscus curvature at the separation line. They also extended their calculations to cases where $\psi > 90°$ by assuming an arc of circle for the meniscus profile between the most upstream place and the separation line, and replacing d by the height of the most upstream point, h_c, and r_c by the radius of curvature there. This arc-of-circle approximation is well supported in the discussion above of Fig. 14. Coyne and Elrod also showed that from their assumption of a parabolic velocity profile it follows that the height of the stagnation line is three times the final film thickness, i.e., $h_s/h_\infty = 3$.

TABLE I

Dependence of h_c/h_∞, r_c/h_c, and h_s/h_∞ on Separation Angle ψ for $N_{Re} = 0$ and $N_{Ca} = 0.125$ ($N = 0.72$) in the Finite Element Calculation

$Q\ (= h_\infty)$	ψ (°)	h_c	h_c/h_∞	r_c	r_c/h_c	h_s	h_s/h_∞
0.13	36.49	0.6822	5.2476	0.3850	0.5595	0.3444	2.649
0.14	51.54	0.7338	5.2414	0.4207	0.5733	0.3709	2.650
0.15	62.46	0.7862	5.2413	0.4562	0.5802	0.3990	2.660
0.16	71.24	0.8394	5.2480	0.4909	0.5847	0.4280	2.675
0.17	78.66	0.8921	5.2480	0.5308	0.5950	0.4600	2.706
0.18	85.05	0.9490	5.2720	0.5833	0.6146	0.4885	2.714

In order to test the validity of Coyne and Elrod's approximations, the results in Table I were extracted from finite element solutions for $N_{Re} = 0$ and $N_{Ca} = 0.125$. The curvature $1/r_c$ ($= 2H$) was calculated as the average of the value from Eq. (18) and the mean value implied by Eq. (19), viz., $N_{Ca}\mathbf{nn} : \mathbf{T}$; the difference between these two estimates proved never to exceed 2% of the average. From Table I it can be seen that h_c/h_∞ and h_s/h_∞ are almost independent of the separation angle ψ, but r_c/h_c is somewhat dependent, changing by 10% as ψ increases from 36.5 to 85.1° in the one case. That the values of h_s/h_∞ are around 2.7 and not 3 is a plain indication that velocity profile departs from parabolic. Coyne and Elrod's approximation and the

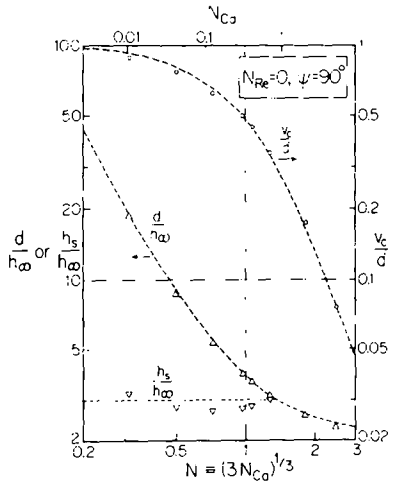

FIG. 15. Dependence of d/h_∞, r_s/d and h_s/h_∞ on N and N_{Ca} for $N_{Re} = 0$ and $\psi = 90°$. Broken lines are Coyne and Elrod's [4] approximate theory.

finite element solutions when the separation angle is 90° are compared in Fig. 15. In the finite element calculations ψ was raised close to 90° by adjusting the flow rate Q, and values for $\psi = 90°$ were extrapolated from the two solutions with separation angles closest to 90°. Finite element solutions which have no stagnation line on the meniscus of course lack points of h_s/h_∞ in Fig. 15. With increasing capillary number the meniscus grows more and more sharply bent near the separation line—the static contact line. The difference between two estimates of curvature at the element there rises from 2 to 5% when $N_{Ca} = 5$ ($N = 2.47$). This means that the result becomes less reliable and a finer tessellation is needed near the static contact line when $N_{Ca} \geqslant 5$; we have not proceeded to refine the finite element mesh in this paper, however. From Fig. 15 the conclusion is that at least when $0.01 \leqslant N_{Ca} \leqslant 5$ Coyne and Elrod's approximation for practical purposes is close enough to the more accurate finite element solutions, so far as meniscus shape is concerned. Evidently their assumption of parabolic velocity profile along spines perpendicular to the meniscus leads to reasonable approximations of meniscus shapes.

By the way, the normal stress, which is balanced by the ambient pressure through the capillary force, is expressed as the sum of normal viscous stress and pressure:

$$T_{nn} = -p + \tau_{nn} = -p + 2\frac{\partial v_n}{\partial n}, \tag{35}$$

where v_n denotes the velocity normal to the free surface and n the distance from it. The pressure contribution, $-p$, and the total T_{nn}, are plotted in Figs. 16a and b. The abscissa is ϕ as shown in Fig. 14a. In both cases the separation angle ψ is less than 90°. However, in Fig. 16b N_{Ca} and Q are smaller giving a wider recirculation zone and higher stress level than those in Fig. 16a. We can see that the normal viscous force is acting inward in the region near the separation line and outward in the region of exponentially thinning film in both cases.

Convergence behavior is shown in Fig. 17 for $N_{Re} = 50$, $N_{Ca} = 0.125$, and five decrements in flow rate Q from 0.3 to 0.13. Iteration at each new value was started from the previous solution. Figure 17a shows that the convergence rate, $\log(\|\Delta\alpha\|_{i+1}/\|\Delta\alpha\|_i)$, where $\|\Delta\alpha\|_i$ is the maximum change of any unknown between the $(i-1)$st and ith iterations, depended strongly on Q in the original formulation. Indeed, as Q decreased the convergence became worse and worse until, below $Q = 0.13$, no domain of convergence could be found and so the calculation came to a halt. The trend was the same as N_{Ca} rose .

Also evident in Fig. 17a is a tendency toward first-order convergence, i.e., the same convergence rate at each iteration, or a straight line in the figure. The asymptotic convergence of Newton iteration is, however, second order (Isaacson and Keller [9], Rheinboldt [15]). But when the Jacobian matrix is not entirely correct, convergence is generally only first order, and the greater the error in the Jacobian, the poorer the convergence rate (Bixler [1]). Figure 17a is *prima facie* evidence that the Jacobian was not complete in Silliman's original formulation.

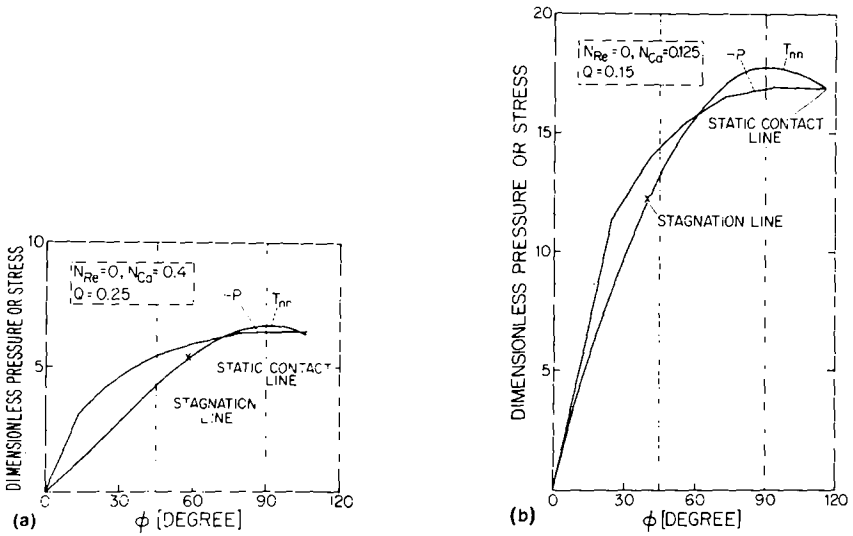

FIG. 16. The variation or pressure, $-p$, and normal stress, $T_{nn} = -p + \tau_{nn}$, versus inclination, ϕ, along the free surface for zero Reynolds number, (a) capillary number, $N_{Ca} = 0.4$ and dimensionless flow rate, $Q = 0.25$, and (b) $N_{Ca} = 0.125$ and $Q = 0.15$.

In contrast, Fig. 17b reveals that the new formulation tends toward second-order convergence, i.e., $\|\Delta\alpha\|_{i+1} < A_i \|\Delta\alpha\|_i^2$, where A_i is a constant with some bounded value. Moreover, second-order convergence is attained at all values of flow rate Q. The conclusion is that the Jacobian matrix is complete and correctly calculated. That this is valuable information is clear from the next section.

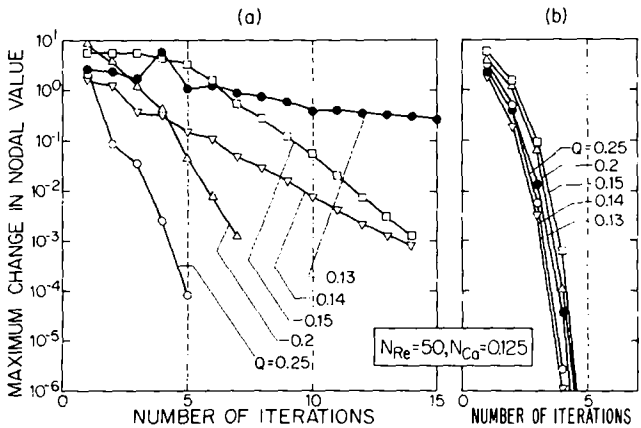

FIG. 17. Convergence behavior of (a) Silliman's formulation and (b) this study, where the complete matrix is used.

6. Sensitivity Coefficients and First-Order Continuation

The wealth of information in the Jacobian matrix of a solution found by Newton iteration is well illustrated by the coefficients of sensitivity of the solution to the parameters, the boundary conditions, or the boundary shape (Silliman and Scriven [22], Brown *et al.* [2]). To review the formulas for sensitivity coefficients with respect to the parameters $\{N_{Re}, N_{Ca}, Q\}$, which are conveniently represented by the vector $\boldsymbol{\pi}$, let the vector $\boldsymbol{\alpha}$ now represent the entire set of unknowns $\{u_i, v_i, p_i, h_i, f_i\}$. Recall that $\mathbf{R}$ is the vector of residuals. The equation set to be solved is

$$\mathbf{R}(\boldsymbol{\alpha}; \boldsymbol{\pi}) = \mathbf{0}. \tag{36}$$

Following Silliman and Scriven [22] we have from the relationship among neighboring solutions

$$d\mathbf{R} = \sum_i \left(\frac{\partial \mathbf{R}}{\partial \alpha_i}\right)_{\pi, \alpha_k; k \neq i} \left(\frac{\partial \alpha_i}{\partial \pi_m}\right)_{\mathbf{R}} + \left(\frac{\partial \mathbf{R}}{\partial \pi_m}\right)_{\alpha, \pi_q; q \neq m} = \mathbf{0} \tag{37}$$

which in matrix form is

$$\mathbf{J}\mathbf{d}_m + \mathbf{s}_m = \mathbf{0}, \tag{38}$$

where $\boldsymbol{d}_m \equiv [\partial \alpha_i / \partial \pi_m]$ is the sensitivity vector of the nodal unknowns and $\mathbf{s}_m \equiv [\partial \mathbf{R} / \partial \pi_m]$ is the sensitivity vector of the residuals.

Because the Jacobian matrix $\mathbf{J}$ is already calculated in the Newton iteration process and $\mathbf{s}_m$ is easily calculated, $\mathbf{d}_m$ can be found with little additional computation. For example, recorded in Fig. 18 is the sensitivity of the pressure at the intersection of the slot wall with the inflow boundary, and of the position of the free surface along the polar arm that is the nearest neighbor to the separation line. The dimensionless pressure at the inflow boundary (which was located at $x = 1$ owing to

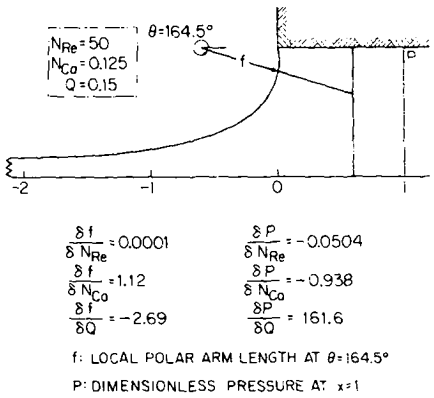

FIG. 18. Sensitivity coefficients evaluated from Jacobian matrix.

the memory capacity available in this calculation, but was still sufficiently upstream that the flow at it is nearly—more than 98% in this case—fully developed) will decrease if Q is reduced or if either N_{Re} or N_{Ca} is increased; it is well to point out that the dimensionless pressure p is related to the dimensional p^* by $p \equiv (d/\mu U)p^*$. In the same circumstances the length of the polar arm will increase further into the slot and the separation angle at the contact line will fall. Given a critical value for the separation angle, one could use the sensitivity coefficients to estimate critical combinations of the parameters N_{Re}, N_{Ca} and Q.

The sensitivity vector is the basis for first-order continuation, a process akin to Euler's method for ordinary differential equations. Continuation provides an improved first estimate to the new solution $\boldsymbol{\alpha}^{(N+1)}$ for parameter values $\boldsymbol{\pi}^{(N+1)}$, given the solution $\boldsymbol{\alpha}^{(N)}$ for parameter $\boldsymbol{\pi}^{(N)}$:

$$\boldsymbol{\alpha}^{(N+1)} = \boldsymbol{\alpha}^{(N)} + \mathbf{d}_m(\pi_m^{(N-1)} - \pi_m^{(N)}). \tag{39}$$

Trial calculations suggest that when parameter values are changed so that no more than six iterations are required for convergence at the level of $\|\Delta\alpha\| < 10^{-4}$, first-order continuation will ordinarily lead to convergence with, on the average, almost one fewer iteration. The optimal combination of continuation and iteration limitation to trace out a curve in parameter space is an open and important issue.

7. Conclusion

The results testify to the value of finding out why an iteration scheme fails to converge, or converging fails to approach its theoretical asymptotic order of convergence. In traditional numerical simulation one "fiddles"—one proceeds by experience, intuition, and trial—to get convergence and often is happy to arrive at any procedure that converges in 10 to 30 iterations from some sort of initial guesses. Convergence behavior is seldom thought worth systematic investigation to understand in terms of available theory. In modern theoretical study and prediction by means of computer-aided functional analysis, as with the subdomain/Galerkin weighted residual method and finite element basis functions, one chooses an analyzed iteration scheme and confirms that it performs as it should, or traces down the reasons it does not. The scheme of choice is Newton iteration, for which it is important to verify that the correct Jacobian is being calculated, by establishing that the iteration approaches second-order convergence, as has now been done.

Research on convergence behavior of Silliman's [23] pioneering finite element analysis of viscous free-surface film flows has led to two major improvements:

1. Combining simple coordinate parametrizations of parts of a free surface, as Cartesian spines and polar spines are combined here, is a convenient way to overcome the breakdown of single coordinate parametrizations, as, for instance, the Cartesian spines employed in Silliman's original formulation, which becomes singular when the meniscus turns through 90° or more. Such a combination not only extends

the accessible parameter range in the study of slot coating, but also makes possible the study of a variety of coating flows such as slide or curtain coating.

2. Employing newly derived general formulas for the derivatives of finite element residuals with respect to free-surface locations along the spines makes possible the calculation of the complete and correct Jacobian matrix for Newton iteration, which not only can lead to much more rapid, second-order convergence, but also provides thereby a criterion for the correctness of the Jacobian of the solution, which contains a wealth of useful information about the solution. The formulas are generally applicable to free-surface and moving boundary situations.

With these improvements the analysis of slot coating has been extended to higher capillary number and lower flow rates (i.e., greater pressure difference applied to oppose the obligatory Couette flow), at which the meniscus becomes more highly bent and the zone of the slow flow and reversed flow grows larger. Interesting features include the variation of the separation angle or contact angle at the line where the meniscus attaches to the corner of the slot; the departure of meniscus profile near that line from an arc-of-circle, which has often been used to approximate it; the location of the stagnation line on the meniscus; the distributions of pressure and viscous normal stress along the meniscus; and the length of the zone of flow relaxation into the asymptotic, fully developed regime downstream. The results show that at high capillary number and low metering rate the meniscus invades into the slot until it would have to make a separation angle that is lower than physically possible; i.e., the meniscus can no longer attach to the slot. This illustrates in a dynamic regime the fact that is already established for the quasi-static meniscus regime: geometric constraints put bounds on meniscus curvature (Higgins and Scriven [7]).

ACKNOWLEDGMENTS

The authors would like to thank Professor R. A. Brown for stimulating discussion about the calculation of the Jacobian matrix by isoparametric mapping, and N. E. Bixler for extensive discussion and valuable insights into finite element analysis of viscous free surface flows and into Newton iteration. The research was supported by the National Science Foundation, Fuji Photo Film Company Ltd., and University of Minnesota Computer Center.

REFERENCES

1. N. E. BIXLER, private communication, 1980.
2. R. A. BROWN, L. E. SCRIVEN, AND W. J. SILLIMAN, *in* "Nonlinear Problems in Dynamics" (P. Holmes, Ed.), SIAM. Philadelphia, 1980.
3. P. W. CHANG, T. W. PATTEN, AND B. A. FINLAYSON, *Comput. Fluids* 7 (1979), 285.
4. J. C. COYNE AND H. G. ELROD, *J. Lubric. Technol. Trans.* ASME **92** (1970), 451; **93** (1971), 156.
5. B. G. HIGGINS AND L. E. SCRIVEN, *Ind. Eng. Chem. Fundam.* **18** (1979), 208.
6. B. G. HIGGINS, PH. D. thesis, University of Minnesota, Minneapolis, 1980.

7. B. G. HIGGINS AND L. E. SCRIVEN, *Chem. Eng. Sci.* **35** (1980), 673.
8. P. HOOD, *Int. J. Num. Methods Eng.* **10** (1976), 379; **11** (1977), 1055.
9. E. ISAACSON AND H. B. KELLER, "Analysis of Numerical Methods," Wiley, New York, 1966.
10. H. S. KHESHGI AND L. E. SCRIVEN, *Bull. Amer. Phys. Soc.* **24** (1979), 1131.
11. L. D. LANDAU AND B. LEVICH, *Acta Physicochim. URSS* **17** (1942), 42.
12. R. E. NICKELL, R. I. TANNER, AND B. CASWELL, *J. Fluid Mech.* **65** (1974), 189.
13. F. M. ORR, Ph. D. thesis, University of Minnesota, Minneapolis, 1976.
14. F. M. ORR AND L. E. SCRIVEN, *J. Fluid Mech.* **84** (1978), 145.
15. W. C. RHEINBOLDT, "Methods for Solving Systems of Nonlinear Equations," SIAM, Philadelphia, 1974.
16. K. J. RUSCHAK, *Chem. Eng. Sci.* **31** (1976), 1057.
17. K. J. RUSCHAK, Preprint 31d 87th National Meeting of AIChE, Boston, 1979.
18. H. SAITO AND L. E. SCRIVEN, *Bull. Amer. Phys. Soc.* **25** (1980), 1101.
19. H. SAITO AND L. E. SCRIVEN, submitted for publication.
20. W. J. SILLIMAN AND L. E. SCRIVEN, *Phys. Fluids* **21** (1978), 2115.
21. W. J. SILLIMAN AND L. E. SCRIVEN, 71st Annual Meeting of AIChE, Miami Beach, 1978.
22. W. J. WILLIAM AND L. E. SCRIVEN, Preprint 31f 87th National Meeting of AIChE, Boston, 1979.
23. W. J. SILLIMAN, Ph. D. thesis, University of Minnesota, Minneapolis, 1979.
24. W. J. SILLIMAN AND L. E. SCRIVEN, *J. Comput. Phys.* **34** (1980), 287.
25. W. J. SILLIMAN AND L. E. SCRIVEN, to be submitted for publication. See also [23].
26. G. STRANG AND G. J. FIX, "An Analysis of the Finite Element Method," Prentice–Hall, Englewood Cliffs, N. J., 1973.
27. R. I. TANNER, R. E. NICKELL, AND R. W. BILGER, *Comput. Methods Appl. Eng.* **6** (1975), 155.
28. R. I. TANNER, "Proceedings, 7th International Congress of Rheology, Gothenburg, Sweden, 1976," p. 140.
29. C. E. WEATHERBURN, "Differential Geometry of Three Dimensions," Cambridge Univ. Press, Cambridge, 1927.